Passivation of nanocrystalline silicon photovoltaic materials employing a negative substrate bias

Chao Wen, Hao Xu, Hong Liu, Zhengping Li and Wenzhong Shen

Institute of Solar Energy, and Key Laboratory of Artificial Structures and Quantum Control (Ministry of Education), Department of Physics and Astronomy, Shanghai Jiao Tong University, Shanghai 200240, People's Republic of China

E-mail: wzshen@sjtu.edu.cn

Abstract

Hydrogenated nanocrystalline silicon (nc-Si:H) shows great promise in the application of third-generation thin film photovoltaic cells. However, the mixed-phase structure of nc-Si:H leads to many defects existing in this important solar energy material. Here we present a new way to passivate nc-Si:H films by tuning the negative substrate bias in plasma-enhanced chemical vapor deposition. Microstructures of the nc-Si:H films prepared under a negative bias from 0 to -300 V have been characterized using Raman, x-ray diffraction, transmission electron microscope, and optical transmission techniques. A novel passivation effect on nc-Si:H films has been identified by the volume fraction of voids in nc-Si:H, together with the electrical properties obtained by electron spin resonance and effective minority lifetime measurements. The mechanism of the passivation effect has been demonstrated by infrared spectroscopy, which illustrates that the high-energy H atoms and ions accelerated by an appropriate bias of -180 V can form more hydrides along the grain boundaries and effectively prevent oxygen incursions forming further Si–O/Si interface dangling bonds in the nc-Si:H films. The detrimental influence of a bias over -180 V on the film quality due to the strong ion bombardment of species with excessively high energy has also been observed directly from the surface morphology by atomic force microscopy.

(Some figures may appear in colour only in the online journal)

1. Introduction

The emergence of semiconductor nanocrystals as the building blocks of nanotechnology has opened up new ways to achieve next-generation solar cells. Hydrogenated nanocrystalline silicon (nc-Si:H) shows great promise in the application of thin film photovoltaic cells due to good features such as a tunable bandgap, strong optical absorption, high carrier mobility, and good stability against light soaking [1–4]. A great deal of attention has been attracted towards the realization of high efficiency, good stability single-junctions [5] and tandem [6, 7] third-generation nc-Si:H thin film solar cells, which are set to make a substantial contribution to the world's photovoltaic market. Recently,

a triple-junction structured cell with an initial active-area efficiency of 16.3% [8] has been demonstrated by taking advantage of nc-Si:H material.

Thin films of nc-Si:H have been grown typically by methods such as plasma-enhanced chemical vapor deposition (PECVD) [9], hot-wire chemical vapor deposition (HWCVD) [10], and radio-frequency (RF) sputtering [11]. Among these methods, PECVD has been established for industrial applications due to its promise to deposit high-quality films uniformly on large-area substrates at low temperature. However, this mixed-phase nc-Si:H material consists of nanometer grains embedded in an amorphous matrix [12], which on the other hand determines that grain boundaries and nanometer-sized voids also exist in nc-Si:H

Table 1. Summary of the physical characteristics of nc-Si:H thin films grown under various DC voltages.

Samples no.	DC bias (V)	Thickness (nm)	X_C (%)	d (nm)	n_∞	N_S (10^{16} cm^{-3})	τ (μs)	C_H (at. %)	C_O (at. %)
DC0	0	735	81.4 ± 4.9	6.5 ± 0.3	2.658	10.2 ± 0.2	44.4 ± 1.3	5.3	8.9
DC50	−50	425	79.5 ± 6.4	5.8 ± 0.2	2.615	11.8 ± 0.5	46.6 ± 2.3	7.6	8.8
DC100	−100	670	75.5 ± 6.8	5.3 ± 0.7	2.690	6.7 ± 0.3	59.9 ± 3.6	8.0	7.6
DC150	−150	600	73.4 ± 5.6	5.1 ± 0.3	2.626	4.2 ± 0.2	63.5 ± 1.3	13.0	1.8
DC180	−180	715	72.3 ± 5.6	4.6 ± 0.5	2.718	3.7 ± 0.3	66.6 ± 3.1	8.6	0.6
DC200	−200	590	69.4 ± 8.3	4.8 ± 0.4	2.636	7.5 ± 0.4	59.2 ± 2.4	11.8	0.3
DC250	−250	700	71.6 ± 4.0	5.7 ± 0.3	2.526	8.8 ± 0.2	47.1 ± 2.6	10.1	0.5
DC300	−300	580	73.3 ± 4.7	7.2 ± 0.6	2.648	9.7 ± 0.6	43.4 ± 1.2	11.3	0.6

films. These grain boundaries and voids take up a certain volume fraction and can induce some unwelcome defects within the nc-Si:H films.

As we know, the formation of nc-Si:H thin films is normally a comprehensive reaction–diffusion process influenced by various factors during the PECVD growth. Previous experiments have shown that ions are important in creating a dense hydrogenated amorphous silicon (a-Si:H) network [13, 14], and the ion energy plays a significant role in determining the transport properties in hydrogenated microcrystalline silicon (μc-Si:H) materials [15]. Hence, applying a direct current (DC) bias on the substrate offers a good way to alter the energy of the ions during the PECVD process, which can optimize the ion bombardment on the growing surface, resulting in device-quality material for the nc-Si:H films.

In this paper, we demonstrate a novel passivation effect on the nc-Si:H thin films by tuning the negative substrate bias in PECVD. We show that film properties such as the crystallinity, the contents of bonded hydrogen and oxygen, and the surface morphology can be effectively controlled by varying the negative bias that accelerates the predominantly positively charged species in the plasma. We discuss the mechanism of the passivation effect of the negative DC bias on the nc-Si:H films through the kinetics of ionic species during the deposition process.

2. Experimental details

The nc-Si:H thin films were grown on both glass and crystalline silicon (c-Si) substrates by a capacitively coupled PECVD system at various DC voltages (0 to −300 V), negatively biased to the stainless steel substrate holder. The PECVD system was operated at an RF of 13.56 MHz, an RF power density of 0.4 W cm^{-2}, a total gas (SiH$_4$ and H$_2$) flow rate of 120 sccm, a chamber pressure of 150 Pa, and a temperature of 250 °C, where the silane (SiH$_4$) content was kept constant at about 1%. The physical characteristics of the nc-Si:H samples are summarized in table 1.

The film thickness was directly measured with a Dektak 6M profilometer. The crystalline volume fraction X_C was calculated from Raman spectra, measured with a Jobin Yvon LabRam HR800 UV micro-Raman spectrometer (backscattering configuration and Ar ion laser at 514.5 nm). The average grain size d was derived from the (111)

x-ray diffraction (XRD) peak, measured with a Bruker D-8 XRD system (Cu Kα radiation, 40 kV and 60 mA), and directly observed by a high-resolution transmission electron microscope (HRTEM, CM200, Philips). The long-wavelength limit of the refractive index n_∞ was deduced from optical transmission spectra, measured with a Jobin Yvon 460 monochromator (400–900 nm spectral range of 0.5 nm resolution). The hydrogen (oxygen) content bonded to silicon C_H (C_O) was obtained from infrared (IR) absorption spectra, measured with a Nicolet Nexus 870 Fourier transform IR (FTIR) spectrometer (400–4000 cm^{-1}). The spin density N_S, characterizing the defect density of the samples, was estimated from electron spin resonance (ESR) measurements, performed with a Bruker EMX-8 ESR spectrometer (X-band, 9.8 GHz and 1 mW). The effective minority carrier lifetime τ was measured using a Semilab PV-2000. The surface morphology of these nc-Si:H films was observed by means of an SII Nanonavi atomic force microscope (AFM). All the comparative data and spectra presented below are normalized by the thickness—such as the spin density, the contents of hydrogen and oxygen, and the FTIR spectra.

3. Results and discussion

For the structural investigation of the nc-Si:H thin films grown under various DC voltages, we carried out micro-Raman and XRD measurements. The typical sample DC50 was chosen to represent all the other samples prepared for investigation. In figure 1(a), we show the Raman spectrum for sample DC50. The experimental Raman spectrum (open circles) can be decomposed into four Gaussian phonon bands (dashed curves) by the strain-incorporated three-dimensional phonon confinement model [16], among which three result from the a-Si phase (longitudinal acoustic (LA) band centered at 300 cm^{-1}, the longitudinal optical (LO) band at 380 cm^{-1}, and the transverse optical (TO$_1$) band at 480 cm^{-1}) and one from the c-Si phase (asymmetric transverse optical (TO$_2$) band at around 520 cm^{-1}). The crystalline volume fraction X_C was about 79.5% for sample DC50, as calculated from $X_C = I_C/(I_C + \gamma I_A)$ [17], where I_C(I_A) is the integrated intensity of the TO$_2$ (TO$_1$) Raman mode and γ is the ratio of the integrated Raman cross section for c-Si to a-Si ($\gamma = 1$ [18]). In figure 1(b), we present the XRD pattern for sample DC50, in which three diffraction peaks appear at $2\theta \sim 29.0°$, 47.5°, and 57.0°, corresponding to the (111), (220), and (311) planes
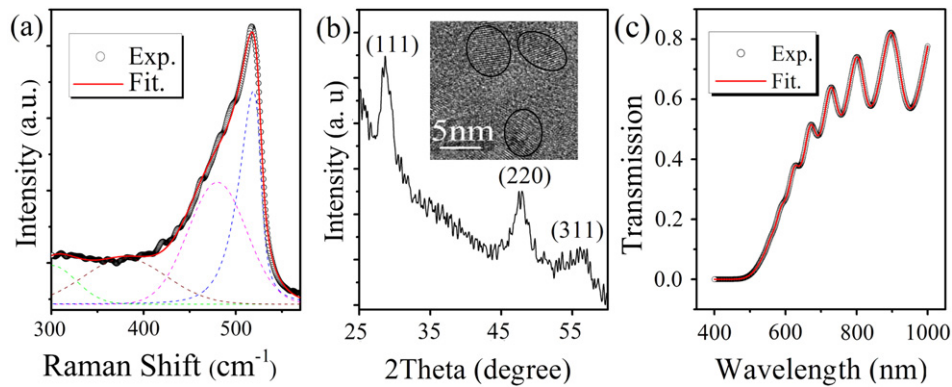
Figure 1. Structural and optical properties of a representative nc-Si:H sample DC50. (a) Experimental (open circles) and fitted (solid curve) Raman spectra. See text for dashed curves. (b) Experimental XRD spectrum. Three diffraction peaks are indicated. An HRTEM image is also shown in the inset. (c) Experimental (open circles) and fitted (solid curve) optical transmission spectra.

of c-Si, respectively. The intensity of the XRD peak for the (111) plane is strongest, indicating that the nanocrystallites have preferentially grown along the (111) direction. The average grain size d for the sample DC50 was calculated to be $\sim$5.8 nm with the Scherrer formula [19], in good agreement with the directly observed value by HRTEM as shown in the inset of figure 1(b).

To obtain optical information on the nc-Si:H samples, we performed optical transmission measurements at room temperature. In figure 1(c), we display experimental (open circles) and fitted (solid curve) optical transmission spectra for sample DC50. From the fitting process within the framework of a modified four-layer-medium transmission model based on the envelope method [20], we obtained both the film thickness ($\sim$420 nm) and the long-wavelength limit of the refractive index ($n_\infty \sim 2.615$). The former value is in good agreement with the directly measured value ($\sim$425 nm) using a step profilometer, as listed in table 1. The latter is an important optical parameter associated with the mass density and atomic structure of nc-Si:H thin films, which together with the crystalline volume fraction X_C from the Raman measurement can be used to calculate the volume fractions of three components (c-Si, a-Si, and voids) in the films [21]. Table 1 lists the structural and optical properties of the nc-Si:H thin films under various DC voltages. From the table, we notice that the crystalline volume fraction X_C varies between 69.4 and 81.4%, and the average grain size d is between 4.6 and 7.2 nm under a negative DC bias from 0 to $-$300 V. Both d and X_C generally decrease from DC0 to DC180, and then increase from DC180 to DC300. That is, the tendencies of d and X_C are similar with the applied bias.

As a mixed-phase material with nanocrystallites embedded in an amorphous matrix, nc-Si:H contains a certain volume fraction of nanometer-sized voids, which should not be neglected when characterizing the microstructure of the films [22]. We have calculated the volume fraction of voids P_V in these nc-Si:H thin films based on Bruggeman's effective media approximation [23] by using the crystalline fraction X_C from the Raman analysis and the refractive index n_∞ from the transmission calculation. As shown in figure 2(a), P_V first decreased when increasing the substrate bias to $-$180 V,
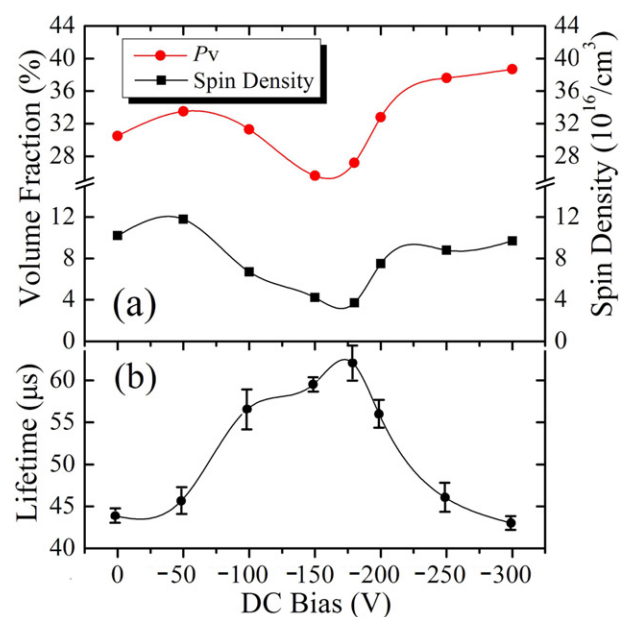
Figure 2. (a) Volume fraction of voids (P_V) and spin density, and (b) effective minority carrier lifetime in nc-Si:H thin films under different DC voltages.

reached its lowest value of around 25.0% between $-$150 and $-$180 V, and then gradually increased to 38.7% when further increasing the substrate bias to $-$300 V. It indicates that films deposited under a DC bias between $-$150 and $-$180 V have a better mass density than the films deposited under other voltages.

Aside from its effect on P_V, the negative DC bias can also alter the defect density within the nc-Si:H films. Many dangling bonds reside on the surface of the voids within the nc-Si:H films. As also illustrated in figure 2(a), the spin density from the ESR measurement, whose evolution tendency is similar to that of P_V, reached its lowest value at $-$180 V. According to the ESR principle, the number of unpaired spins is positively proportional to the density of neutral dangling bonds. Therefore, the ESR results in figure 2(a) reveal that the defect density in nc-Si:H reached

its lowest value in the film deposited at −180 V. This agreement of the thin film quality with the applied bias can be further supported by the direct measurement of the effective minority carrier lifetime τ shown in figure 2(b), where the film with the lowest density of dangling bonds under −180 V has the highest minority carrier lifetime. Therefore, it can be identified that an appropriate negative DC bias has a passivation effect on the nc-Si:H films, and can help to deposit a good quality film with dense structure as well. We should notice that for the typical nc-Si:H films deposited by PECVD, an amorphous seed layer with a thickness less than about 20 nm will grow first on the substrate. The properties of PECVD deposited films with thicknesses of dozens of nanometers can change remarkably with changing thickness. However, the thicknesses ranging from about 500 to 700 nm in our samples are much greater than 20 nm, in which case the properties of the nc-Si:H films mainly depend on the deposition technology. As a result, the difference in the thicknesses from about 500 to 700 nm will not affect how the applied negative bias changes the properties of the samples.

During the deposition process, the kinetic energy of ionic species such as H ions and SiH$_x$ radicals can be greatly affected by the applied substrate bias, which can further result in changes of the film properties. Of these ionic species, H ions take up an overwhelming volume in the high H$_2$ dilution profiling, which can be accelerated by the negative DC bias towards the growing film. These accelerated H ions can affect the defect densities as well as the oxygen content in the films by incorporating with the dangling bonds inside the film to form certain types of hydrides with different bonding configurations, which is an important factor for the passivation effect of the DC bias. Therefore, to better understand the mechanism of the passivation effect, we have performed IR-transmission measurements, which can give detailed information about the H and O contents bonded to Si (C_H and C_O), as well as the Si–H and Si–O bonding configurations of the films prepared under different DC voltages.

We show in figure 3 the IR absorption results of these nc-Si:H thin films. Each spectrum exhibits four absorption peaks, including three Si–H peaks in the rocking–wagging, bending, and stretching modes centered around 630, 880, and 2090 cm^{-1}, respectively [24, 25], and one Si–O peak in the stretching mode centered at 1000–1200 cm^{-1} [26, 27]. It is found that the hydrogen absorption centered at 630 cm^{-1}, used to obtain the bonded-hydrogen content [24, 28], increased gradually with the substrate bias from 0 to −300 V, while the oxygen absorption centered at 1000–1200 cm^{-1} decreased in the meantime. The observation of the Si–O peak indicates the incorporation of oxygen in the samples. The bonded-hydrogen content C_H has been calculated by numerical integration from the absorption peak of the Si–H wagging mode at around 630 cm^{-1} in figure 3 using the formula $C_H = 1/N_{Si} \times A_W \times \int (\alpha(\nu)/\nu)\mathrm{d}\nu$, where $\alpha(\nu)$ is the absorption coefficient, ν the wavenumber, $N_{Si} = 5 \times 10^{22}$ cm^{-3} the atomic density of the c-Si, and $A_W = 2.1 \times 10^{19}$ cm^{-2} the proportionality constant [29]. Meanwhile, the bonded oxygen content C_O can be similarly obtained
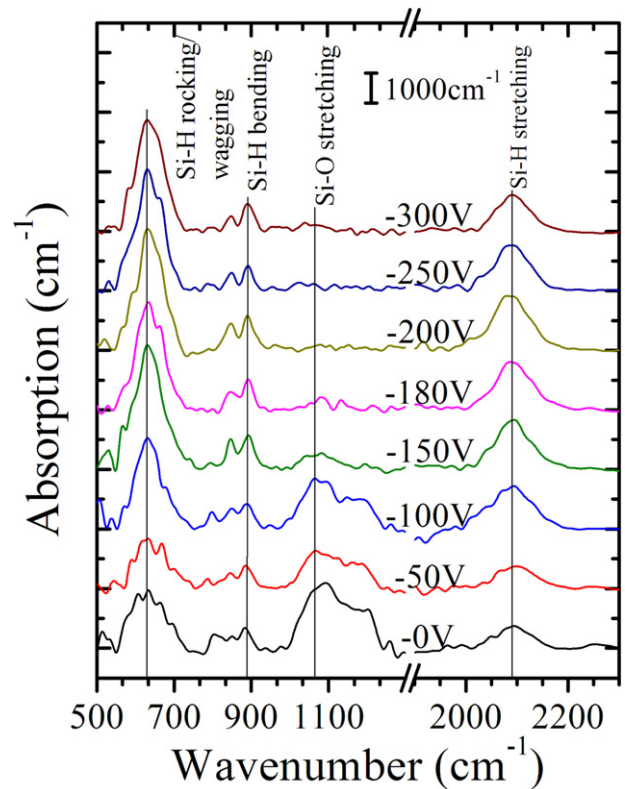

Figure 3. IR absorption spectra of nc-Si:H thin films under various DC voltages. Each spectrum is vertically shifted for clarity.

from numerical integration of the Si–O stretching mode at 1000–1200 cm^{-1} with $A_W = 2.8 \times 10^{19}$ cm^{-2} [25, 26]. The deduced C_H and C_O values for all the nc-Si:H films have been listed in table 1.

From the yielded C_H and C_O listed in table 1, it is clear that there is inverse correlation between C_H and C_O in these nc-Si:H films. Although similar behavior was found by other groups [30, 31], no further investigations have been carried out with a convincing explanation about this inverse correlation. The oxygen incursions caused by post-deposition oxidation of the grain boundary can result in an increase of dangling bonds in the nc-Si:H films [32], probably in the formation of the Si–O/Si interface dangling bonds (P$_b$ center defects) [33]. On the other hand, hydrogen makes a positive contribution to prevent the unwelcome oxygen incursions by saturating dangling bonds along the grain boundaries of the nc-Si:H films. This fraction of hydrogen along the grain boundaries can form hydrides with a certain type of bonding configuration, as shown in figure 4(a).

As mentioned in figure 3, the absorption peak at around 2090 cm^{-1} stands for the stretching mode of Si–H, whose frequency position depends on the unscreened eigenfrequency of the hydride, bulk screening, local hydride density, and possible mutual dipole interactions in the hydrogen incorporation configuration [34]. We have identified in figure 4(a) the five different bonding configurations of hydrides by the fine structures of the stretching mode peak: the low stretching mode (LSM) at 1980–2010 cm^{-1}, the middle stretching mode (MSM) at ∼2033 cm^{-1}, the
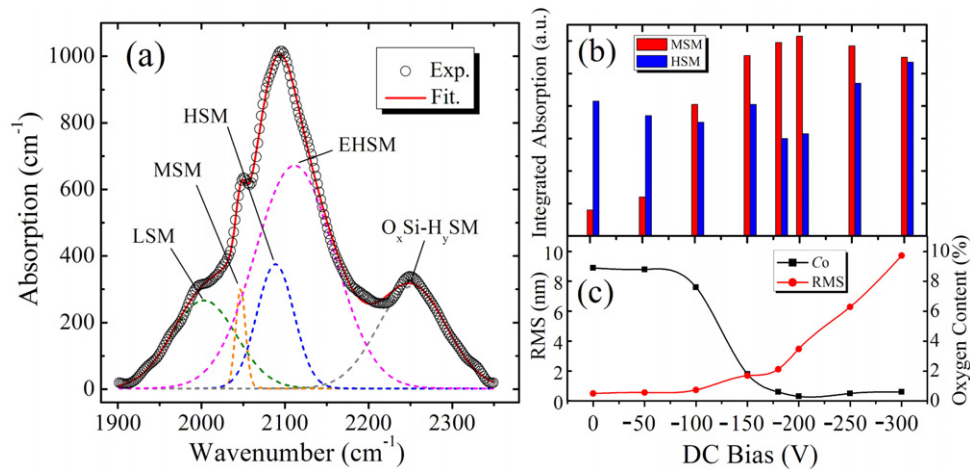
Figure 4. (a) A close-up of the IR absorption spectrum for the Si–H stretching mode of a representative sample DC50. The solid curve represents the total fit and the five dashed curves are Gaussian-shaped stretching modes as labeled. (b) Bar graph of the integrated absorption intensity for HSM and MSM in nc-Si:H thin films under different DC voltages. (c) Oxygen content (C_O) and surface root-mean-square roughness of nc-Si:H thin films under different DC voltages.

high stretching mode (HSM) at 2070–2100 cm^{-1}, the extreme high stretching mode (EHSM) at 2140–2150 cm^{-1}, and the oxygen-related stretching mode ($O_xSi–H_y$ SM) at $\sim$2250 cm^{-1}. The physical origin and interpretation of these modes have been the subjects of many investigations. The LSM and HSM originate from the a-Si:H tissue of the nc-Si:H thin films, where the monohydrides in vacancies contribute dominantly to the LSM, while both the monohydrides and the dihydrides on void surfaces contribute significantly to the HSM [35]. Reports claimed that the distinction between the LSM and the HSM can be attributed to the hydride type and the bulk environment in which it resides [24, 35, 36]. The additional MSM existing only in nc-Si:H rather than a-Si:H [37–40] is due to the vibration of hydrides in a platelet-like configuration at the amorphous–crystalline interfaces, i.e., the grain boundaries [40–42]. The EHSM is related to the trihydrides of the films deposited under high hydrogen dilution conditions [41]. The mode of the $O_xSi–H_y$ SM corresponds to the hydride $O_xSi–H_y$ vibration with oxygen atoms back-bonded to the silicon atoms [43], which together with the Si–O stretching mode at 1000–1200 cm^{-1}, can reflect the bulk oxidation of the film.

Among the five bonding configurations of hydrides, the MSM and HSM are the two main modes that can determine the mechanism of the passivation effect. The former mode corresponds to the bonding configuration of the hydrides in the grain boundaries, which can effectively passivate the nc-Si:H films by preventing oxygen incursions from inducing an increase of dangling bonds (P_b center defects) [33]. The latter one is related to the bonding configuration of the hydrides on the void surfaces, which can reflect the density of the nc-Si:H films. In figure 4(b), we have illustrated the integrated intensities of the MSM and HSM for all the samples DC0–DC300, indicating the changes of hydrogen-bonding configurations in the grain boundaries and on the void surfaces, respectively. It is clear that the integrated intensity of the MSM increased with the bias from 0 to −180 V, and

generally remained unchanged at high values when further increasing the bias from −180 to −300 V. This observation indicates that H atoms and ions in the plasma have been accelerated by the increased bias to diffuse into the growing film with a higher kinetic energy and passivate more dangling bonds, which results in the formation of more hydrides along the grain boundaries. In contrast, the evolution of the HSM integrated intensity shows a slight decrease from 0 to −180 V, and then gradually increased with the bias from −180 to −300 V. This phenomenon has suggested that the film deposited under the bias of −180 V has a compact structure with the lowest void fraction, which agrees well with the results of P_V in figure 2(a).

Based on the above investigation, we can hereby draw a clear physical picture for the mechanism of the passivation effect of the negative DC bias in the deposition of nc-Si:H thin films. In the low range of negative substrate bias, ions were accelerated to an increasing kinetic energy as the bias increased gradually from 0 to −180 V. Those accelerated ions transferred more energy to the growth surface and thus enhanced the diffusion length of the SiH_x ($x =$ 0–3, mainly for $x = 3$) precursors. After these precursors preferentially attached to the energetic favorable growing sites, an atomically more ordered film structure with a lower void fraction was formed, resulting in a decrease of P_V from 0 to −180 V as presented in figure 2(a). Furthermore, higher energy H atoms and ions led to deeper H penetration into the growing film and the formation of more hydrides along the grain boundaries, as illustrated by the evolution of the integrated intensity of the MSM in figure 4(b). Consequently, this process effectively passivated the dangling bonds along the grain boundaries, and thus lowered the defect density of the films by preventing the probability of the post-deposition oxidation of the films forming further Si–O/Si interface dangling bonds (P_b centered). This is also in agreement with the decreased evolution of C_O shown in figure 4(c) from 0 to −180 V.
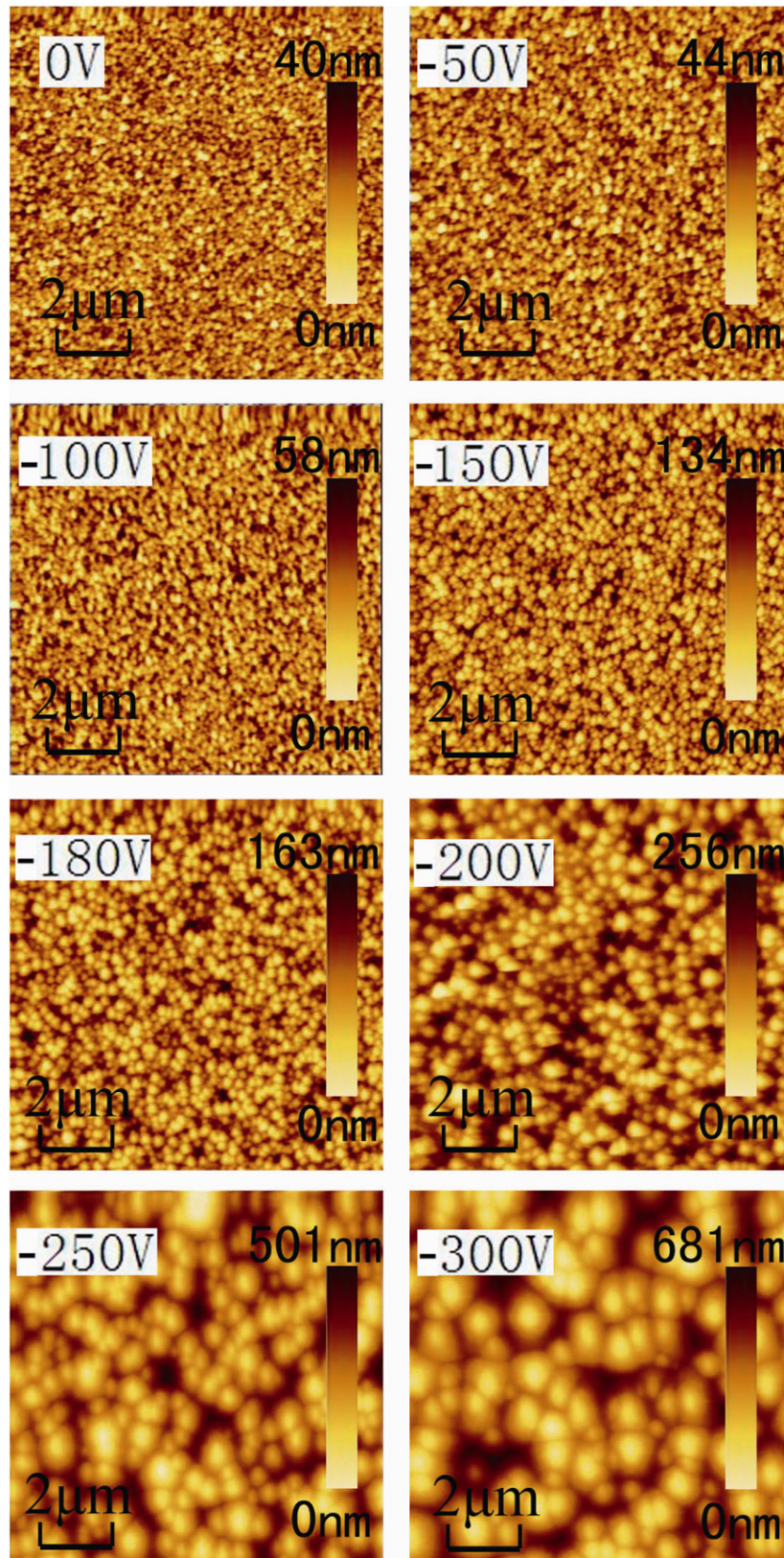
Figure 5. AFM images of nc-Si:H thin films, showing a surface morphology change by the negative DC bias.

While further increasing the substrate bias from -180 gradually to -300 V, the strong ion bombardment of species with excessively high kinetic energy has become detrimental for the growing film. The evolution of C_O shown in figure 4(c) remained almost unchanged at low values from -180 to -300 V. However, the defect density increased in this bias

range, as illustrated in figure 2(a), which is due to the remarkably degraded surface morphology of the films. In this condition, the H species were accelerated to a much greater magnitude than other radicals in the plasma, and therefore the involvement of heavy SiH_x radicals in the plasma can be neglected. H atoms and ions on the growing surface with excessively high kinetic energies enhanced the H-abstraction reaction, which reduced the surface diffusion length of film precursors [44, 45]. This has led to not only an increase in the volume fraction of voids P_V within the film [46] (see figure 2(a)), but also a degraded surface morphology as shown in figure 5.

Noticeably, there is a significant difference in the changes of the surface morphology in figure 5 between the bias range from 0 to −180 V and the range from −180 to −300 V. The evolution of the root-mean-square (RMS) used for the characterization of the mean surface roughness is plotted in figure 4(c), showing that the RMS increased much faster in the bias range −180 to −300 V compared with the range 0 to −180 V. The dramatic morphology change can be explained in terms of the surface diffusion length of the film precursors (SiH_x). H atoms and ions with high kinetic energies on the growing surface enhanced the H-abstraction reaction, leading to a reduction in the surface diffusion length of SiH_x [44, 45]. Thus, the film precursors tended to pile up instead of reaching their favorable growing sites and formed a degraded morphology on the growing surface with higher RMS when increasing the substrate bias, especially in the range from −180 to −300 V.

Considering the high integrated intensity of the MSM and the almost unchanged C_O at low values in the −180 to −300 V bias range, the H atoms and ions could still permeate deep into the growing film and passivate the films by saturating most of the dangling bonds along the grain boundaries, effectively preventing oxygen incursions from forming Si–O/Si interface dangling bonds (P_b centered). However, more dangling bonds were formed on the degraded surfaces. The enhancement of the H-abstraction reaction removed a fraction of passivating H on the surface and created excess surface unpassivated dangling bonds, which together with the degraded surface morphology dominates the increase of the defect density in this high bias range. Apparently, further increasing the substrate bias over −180 V becomes detrimental to the quality of the growing films.

4. Conclusion

In summary, a novel passivation effect has been demonstrated in the important solar energy material of nc-Si:H thin films by tuning the negative substrate bias from 0 to −300 V in PECVD. We have employed Raman, XRD, TEM, and optical transmission techniques for the microstructure characterization of nc-Si:H thin films. The good agreement among the volume fraction of voids, the spin density, and the effective minority lifetime has evidenced that the nc-Si:H film deposited under −180 V has good quality with the most compact structure containing the lowest defect density. From detailed information on the bonding configurations in the IR

absorption spectroscopy, a full explanation has been provided for the mechanism of the passivation effect. The accelerated H atoms and ions with moderate energy under −180 V can form more hydrides along the grain boundaries, effectively passivating the dangling bonds and preventing the oxygen incursions from forming further Si–O/Si interface dangling bonds. The excessively high energies of ions accelerated by bias values over −180 V become detrimental to the quality of the growing films due to the strong ion bombardment effect, as also revealed from the AFM observation of the film surface morphology. The present work opens a new way for the deposition of device-quality nc-Si:H films suitable for application in third-generation thin film photovoltaic cells.

References

[1] Kitao J, Harada H, Yoshida N, Kasuya Y, Nishio M, Sakamoto T, Itoh T, Nonomura S and Nitta S 2001 Absorption coefficient spectra of μc-Si in the low-energy region 0.4–1.2 eV *Sol. Energy Mater. Sol. Cells* **66** 245–51

[2] Zhang R, Chen X Y, Zhang K and Shen W Z 2006 Photocurrent response of hydrogenated nanocrystalline silicon thin films *J. Appl. Phys.* **100** 104310

[3] Chen X Y, Shen W Z and He Y L 2005 Enhancement of electron mobility in nanocrystalline silicon/crystalline silicon heterostructures *J. Appl. Phys.* **97** 024305

[4] Keppner H, Meier J, Torres P, Fischer D and Shah A 1999 Microcrystalline silicon and micromorph tandem solar cells *Appl. Phys.* A **69** 169–77

[5] Mai Y, Klein S, Geng X and Finger F 2004 Structure adjustment during high-deposition-rate growth of microcrystalline silicon solar cells *Appl. Phys. Lett.* **85** 2839–41

[6] Yang J, Yan B and Guha S 2005 Amorphous and nanocrystalline silicon-based multi-junction solar cells *Thin Solid Films* **487** 162–9

[7] Yamamoto K *et al* 2005 A thin-film silicon solar cell and module *Prog. Photovolt. Res. Appl.* **13** 489–94

[8] Yan B, Yue G, Sivec L, Yang J, Guha S and Jiang C-S 2011 Innovative dual function nc-SiO$_x$:H layer leading to a >16% efficient multi-junction thin-film silicon solar cell *Appl. Phys. Lett.* **99** 113512

[9] Edelberg E, Bergh S, Naone R, Hall M and Aydil E S 1996 Visible luminescence from nanocrystalline silicon films produced by plasma enhanced chemical vapor deposition *Appl. Phys. Lett.* **68** 1415–7

[10] Fonrodona M, Soler D, Escarré J, Villar F, Bertomeu J, Andreu J, Saboundji A, Coulon N and Mohammed-Brahim T 2006 Low temperature amorphous and nanocrystalline silicon thin film transistors deposited by hot-wire CVD on glass substrate *Thin Solid Films* **501** 303–6

[11] Gonçalves C, Charvet S, Zeinert A, Clin M and Zellama K 2002 Nanocrystalline silicon thin films prepared by radio frequency magnetron sputtering *Thin Solid Films* **403/404** 91–6

[12] He Y, Yin C, Cheng G, Wang L, Liu X and Hu G Y 1994 The structure and properties of nanosize crystalline silicon films *J. Appl. Phys.* **75** 797–803

[13] Drevillon B, Perrin J, Siefert J M, Huc J, Lloret A, de Rosny G and Schmitt J P M 1983 Growth of hydrogenated amorphous silicon due to controlled ion bombardment from a pure silane plasma *Appl. Phys. Lett.* **42** 801–3

[14] Hamers E A G, van Sark W G J H M, Bezemer J, Meiling H and van der Weg W F 1998 Structural properties of a-Si:H related to ion energy distributions in VHF silane deposition plasmas *J. Non-Cryst. Solids* **226** 205–16

[15] Kondo M, Fukawa M, Guo L and Matsuda A 2000 High rate growth of microcrystalline silicon at low temperatures *J. Non-Cryst. Solids* **266–269** 84–9 Part 1

[16] Yang M, Huang D, Hao P, Zhang F, Hou X and Wang X 1994 Study of the Raman peak shift and the linewidth of light-emitting porous silicon *J. Appl. Phys.* **75** 651–3

[17] Bustarret E, Hachicha M A and Brunel M 1988 Experimental determination of the nanocrystalline volume fraction in silicon thin films from Raman spectroscopy *Appl. Phys. Lett.* **52** 1675–7

[18] Droz C, Vallat-Sauvain E, Bailat J, Feitknecht L, Meier J and Shah A 2004 Relationship between Raman crystallinity and open-circuit voltage in microcrystalline silicon solar cells *Sol. Energy Mater. Sol. Cells* **81** 61–71

[19] Fitzsimmons M R, Eastman J A, Müller-Stach M and Wallner G 1991 Structural characterization of nanometer-sized crystalline Pd by x-ray-diffraction techniques *Phys. Rev.* B **44** 2452–60

[20] Chen H, Gullanar M H and Shen W Z 2004 Effects of high hydrogen dilution on the optical and electrical properties in B-doped nc-Si:H thin films *J. Cryst. Growth* **260** 91–101

[21] Müllerová J, Šutta P, van Elzakker G, Zeman M and Mikula M 2008 Microstructure of hydrogenated silicon thin films prepared from silane diluted with hydrogen *Appl. Surf. Sci.* **254** 3690–5

[22] Moss S C and Graczyk J F 1969 Evidence of voids within the as-deposited structure of glassy silicon *Phys. Rev. Lett.* **23** 1167–71

[23] Bruggeman D A G 1935 Berechnung verschiedener physikalischer Konstanten von heterogenen Substanzen. I. Dielektrizitätskonstanten und Leitfähigkeiten der Mischkörper aus isotropen Substanzen *Ann. Phys., Lpz.* **416** 636–64

[24] Brodsky M H, Cardona M and Cuomo J J 1977 Infrared and Raman spectra of the silicon-hydrogen bonds in amorphous silicon prepared by glow discharge and sputtering *Phys. Rev.* B **16** 3556–71

[25] Lucovsky G, Nemanich R J and Knights J C 1979 Structural interpretation of the vibrational spectra of a-Si:H alloys *Phys. Rev.* B **19** 2064–73

[26] Freeman E C and Paul W 1978 Infrared vibrational spectra of rf-sputtered hydrogenated amorphous silicon *Phys. Rev.* B **18** 4288–300

[27] Tsu D V, Lucovsky G and Davidson B N 1989 Effects of the nearest neighbors and the alloy matrix on Si–H stretching vibrations in the amorphous SiO_r:H $(0 < r < 2)$ alloy system *Phys. Rev.* B **40** 1795–805

[28] Kroll U, Meier J, Shah A, Mikhailov S and Weber J 1996 Hydrogen in amorphous and microcrystalline silicon films prepared by hydrogen dilution *J. Appl. Phys.* **80** 4971–5

[29] Langford A A, Fleet M L, Nelson B P, Lanford W A and Maley N 1992 Infrared absorption strength and hydrogen content of hydrogenated amorphous silicon *Phys. Rev.* B **45** 13367–77

[30] Hugger P G, Cohen J D, Yan B, Yue G, Yang J and Guha S 2010 Relationship of deep defects to oxygen and hydrogen content in nanocrystalline silicon photovoltaic materials *Appl. Phys. Lett.* **97** 252103

[31] Kočka J, Stuchlíková H, Ledinský M, Stuchlík J, Mates T and Fejfar A 2009 Microcrystalline silicon, grain boundaries and role of oxygen *Sol. Energy Mater. Sol. Cells* **93** 1444–7

[32] Xu L, Li Z P, Wen C and Shen W Z 2011 Bonded hydrogen in nanocrystalline silicon photovoltaic materials: impact on structure and defect density *J. Appl. Phys.* **110** 064315

[33] Finger F, Carius R, Dylla T, Klein S, Okur S and Gunes M 2003 Stability of microcrystalline silicon for thin film solar cell applications *IEE Proc. Circuits, Devices and Systems* **150** 300–8

[34] Smets A H M and van de Sanden M C M 2007 Relation of the Si–H stretching frequency to the nanostructural Si–H bulk environment *Phys. Rev.* B **76** 073202

[35] Smets A H M, Kessels W M M and van de Sanden M C M 2003 Vacancies and voids in hydrogenated amorphous silicon *Appl. Phys. Lett.* **82** 1547–9

[36] Ouwens J D and Schropp R E I 1996 Hydrogen microstructure in hydrogenated amorphous silicon *Phys. Rev.* B **54** 17759–62

[37] Vignoli S, Fontcuberta i Morral A, Butté R, Meaudre R and Meaudre M 2002 Hydrogen related bonding structure in hydrogenated polymorphous and microcrystalline silicon *J. Non-Cryst. Solids* **299–302** 220–5 Part 1

[38] Agarwal S, Hoex B, van de Sanden M C M, Maroudas D and Aydil E S 2004 Hydrogen in Si–Si bond center and platelet-like defect configurations in amorphous hydrogenated silicon *J. Vac. Sci. Technol.* B **22** 2719–26

[39] Fujiwara H, Kondo M and Matsuda A 2002 Microcrystalline silicon nucleation sites in the sub-surface of hydrogenated amorphous silicon *Surf. Sci.* **497** 333–40

[40] Lebib S and Roca i Cabarrocas P 2005 Effects of ion energy on the crystal size and hydrogen bonding in plasma-deposited nanocrystalline silicon thin films *J. Appl. Phys.* **97** 104334

[41] Marra D C, Edelberg E A, Naone R L and Aydil E S 1998 Silicon hydride composition of plasma-deposited hydrogenated amorphous and nanocrystalline silicon films and surfaces *J. Vac. Sci. Technol.* A **16** 3199–210

[42] von Keudell A and Abelson J R 1998 The interaction of atomic hydrogen with very thin amorphous hydrogenated silicon films analyzed using *in situ* real time infrared spectroscopy: reaction rates and the formation of hydrogen platelets *J. Appl. Phys.* **84** 489–95

[43] Niwano M, Kageyama J-I, Kurita K, Kinashi K, Takahashi I and Miyamoto N 1994 Infrared spectroscopy study of initial stages of oxidation of hydrogen-terminated Si surfaces stored in air *J. Appl. Phys.* **76** 2157–63

[44] Mahan A H, Xu Y, Williamson D L, Beyer W, Perkins J D, Vanecek M, Gedvilas L M and Nelson B P 2001 Structural properties of hot-wire a-Si:H films deposited at rates in excess of 100 Å/s *J. Appl. Phys.* **90** 5038–47

[45] Robertson J 2000 Deposition mechanism of hydrogenated amorphous silicon *J. Appl. Phys.* **87** 2608–17

[46] Saha S C, Barua A K and Ray S 1993 The role of hydrogen dilution and radio frequency power in the formation of microcrystallinity of n-type Si:H thin film *J. Appl. Phys.* **74** 5561–8